

Rigid Band Doping of Large-Pore Semiconducting Graphene Nanomeshes

Mohamed S. Eldeeb,¹ Mohamed M. Fadlallah,^{1,2}

Glenn J. Martyna,³ and Ahmed A. Maarouf^{4,1}

¹*Center for Fundamental Physics, Zewail City of Science and Technology, Giza 12588, Egypt*

²*Department of Physics, Faculty of Science, Benha University, Benha, Egypt*

³*IBM T. J. Watson Research Center, Yorktown Heights, NY 10598*

⁴*Egypt Nanotechnology Research Center & Department of Physics,*

Faculty of Science, Cairo University, Giza, Egypt 12613

(Dated: February 25, 2019)

Abstract

Porous graphene structures, also termed graphene nanomeshes (GNMs), are gaining increasing interest due to potential applications, for example, chemical sensing, ion-filtration, and nanoelectronics. Semiconducting GNMs can have fractional eV band gaps, which makes them good candidates for graphene-based electronics, provided that a mechanism for their stable and controlled doping is found. Recent work has shown that controlled passivation of the edges of difficult to controllably fabricate subnanometer pores and subsequent doping by atoms or molecules gives rise to *p*- and *n*-doped GNM structures. Here, we use first principle calculations to study the effect of the pore size on the doping physics of GNM structures with larger pores that can potentially host more than a single dopant. We show that such a mechanism works even for pores with relatively large radius. We also study the effect of the number of dopants per pore on doping stability. We find that stable rigid band doping occurs in such structures even if the dopants form a nano-cluster in the pore. Rigid-band doping is achieved in all *n*- and *p*-doping studied.

I. INTRODUCTION

Over the last 15 years, graphene has captured the interest of both theoretical and experimental researchers due to its unique physical and chemical properties, leading to its potential application to many technological niches including chemical separation,¹ nanocatalysis,² RF amplifiers,³ and nanoelectronics.^{4–6} Despite its high electronic mobility,⁷ graphene lacks an electronic gap, which limits its potential as a substitute for silicon in the transistor world.

Graphene nanomeshes (GNM's, also called porous graphene) are formed by creating a superlattice of pores in a graphene sheet. Depending on the superlattice constant and the pore geometry, these structures can inherit graphene's semimetallicity, or can be semiconducting with a fractional eV gap.^{8–15} If such semiconducting structures can be controllably and stably doped, they can be used to fabricate graphene-based computer logic switches and spintronic devices.¹⁶

Controlled, stable, chemical doping of pore-edge passivated GNM's has been recently proposed:¹⁷ A neutral dopant undergoes a charge transfer reaction with the GNM of specific pore edge passivation, ionizes, and is then electrostatically trapped in the pore by the local dipole moments of the edge functional groups. The charge so transferred dopes the GNM, moving the Fermi level into the valence or the conduction bands (see Fig. 1). The GNM band structure is essentially not affected by the doping process, and the dopant state involved in the charge transfer is far from the Fermi level. In this way, a stable controlled rigid band doping of semiconducting GNM is achieved.¹⁷

GNMs have been fabricated by several groups, with pore-size distributions in the 3-200 nm range.^{18–21} A study of the I-V characteristics of *p*-doped GNM-based transistors indicated that their ON-OFF ratio was an order of magnitude larger than that of pristine graphene, but with lower electrical conductivity. Most recently, sub nanometer pores were fabricated, albeit without the periodicity necessary for transport application.²² Since fabrication techniques are likely to yield GNM's with nanometer-sized pores which can host more than one dopant atom, a question arises regarding the dopant stability in the pores. How would multiple dopants behave in a large pore? Would they uniformly distribute around the pore edge, or would they cluster together, with obvious impact on the dopants binding energy? In addition, how would the distribution/clustering of the dopants in the pore affect the rigid band doping picture?

In this work, we attempt to answer the aforementioned questions through the study of the electronic properties of a representative set of GNM structures with varying pore sizes, dopant loads, and pore edge passivations, for both *n*- and *p*-doping. Using first principles calculations, we will calculate the binding energy as well as the maximum number of dopants bound per pore. We will also explore the effect of multiple small dopants on the band structure of the doped GNMs to determine whether or not the rigid band picture is applicable.

II. DESCRIPTION OF THE PHYSICAL SYSTEM

Since *n*- and *p*-type FET's are required for digital electronics, the adoption of GNM's for post-CMOS technologies relies heavily on a thorough understanding of their properties, including doping. Experimental work on GNM's currently achieves pore diameters as small as 3 nm.²⁰ Therefore, we have to consider multiple dopants per pore, studying the details of their packing and stability for near term applications. This also provides a framework for understanding the behavior of dopant ionic complexes.

We recently suggested a novel doping approach¹⁷ to dope GNM's based on a concept from chemistry, ion chelation. Here, the pore perimeter is passivated by a species with an electronegativity different from carbon, which results in the formation of local radial dipoles at the pore perimeter creating a favorable environment in which to host ions. A neutral atom is ionized by the sheet through a charge transfer reaction in which the electrostatic energy gain is higher than the charge transfer cost. This results in the tight electrostatic binding of the ion, and the rigid band doping of the GNM sheet. This is consistent with the behavior predicted by the Newns-Anderson and Norskov-type models.²³⁻²⁵ The pore lattice strictly controls dopant concentration. In the following, we build on this basic physics.

In GNMs with nanometer-sized pores, electrostatic dopant binding is expected to decrease due to three effects: 1- A weaker interaction between a dopant and the pore dipoles. 2- The increase in the charge transfer to the sheet, and hence its energy cost. 3- The repulsion between ionized dopants. 4- The introduction of more dopants in large pores can lead to the clustering of dopant atoms. This implies that chemical binding, well known in metals, may occur between the dopant atoms which may affect the doping physics observed with single dopants (Fig. 1).

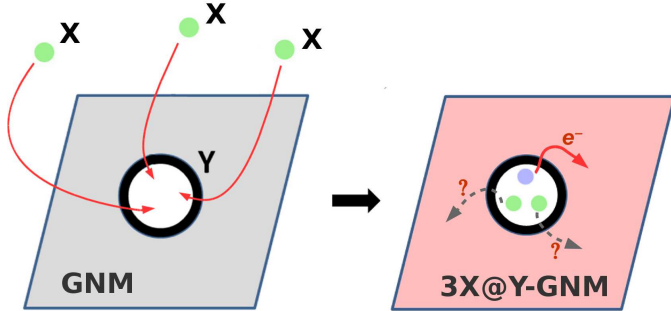


FIG. 1: A conceptual sketch of multiple-ion chelation doping of a GNM. Chelant atoms are successively brought close to pore, where some or all of them become ionized, thus doping the GNM. Here, *n*-doping is shown; *p*-doping simply replaces the electron with a hole. In principle, partial charge transfer can occur, where the HOMO/LUMO of the chelants can move relative to the GNM spectrum.^{24,26,27}

In order to understand the implications of these effects on the doping of GNMs, we study the doping produced by multiple dopants in *n*- and *p*-doped GNM systems: For *n*-type, we consider an oxygen passivated GNM, for two supercell and two pore sizes. We study the *n*-doping of this GNM by multiple lithium and sodium atoms. For *p*-type, we consider a hydrogen passivated GNM, also for two supercell and two pore sizes. The dopants in that case are multiple fluorine and chlorine atoms.

We use density functional theory within the generalized gradient approximation to describe the systems of interest as verified in Ref.[17]. We introduce the nomenclature *nX@Y-GNM_c* to denote a GNM structure with a supercell size of *c* graphene unit cells, with its pore edges passivated by species "Y", and with *n* atoms of species "X" hosted in the pore. Therefore, our parameter space is constructed by X = {Li,Na}, *n* = 1, 2, ..6, and *c* = 9, 12 for the O-GNM systems, and X = {F,Cl}, *n* = 1, 2, ..6, and *c* = 9, 12 for the H-GNM systems. We will cover points in this parameter space that are sufficient to unravel the doping physics.

III. RESULTS AND DISCUSSION

We begin by presenting the electronic properties of our undoped GNM systems. In Fig.2(a,b), the insets show an oxygen- and a hydrogen-passivated GNM, with supercell size

of 9×9 graphene unit cells (O-GNM9 and H-GNM9), as well as their density of states (DOS). The two GNMs have a pore size of about 0.8 nm, and are chemically stable as the passivation saturates all bonds. Both GNMs are semiconducting with a gap of about 0.5 eV for the oxygen case, and 0.7 eV for the hydrogen case. Projection of the DOS on the atomic orbitals (PDOS) shows that the states of the passivating species are located far from the top/bottom of the valence/conduction bands, and are therefore not expected to induce resonant scattering.

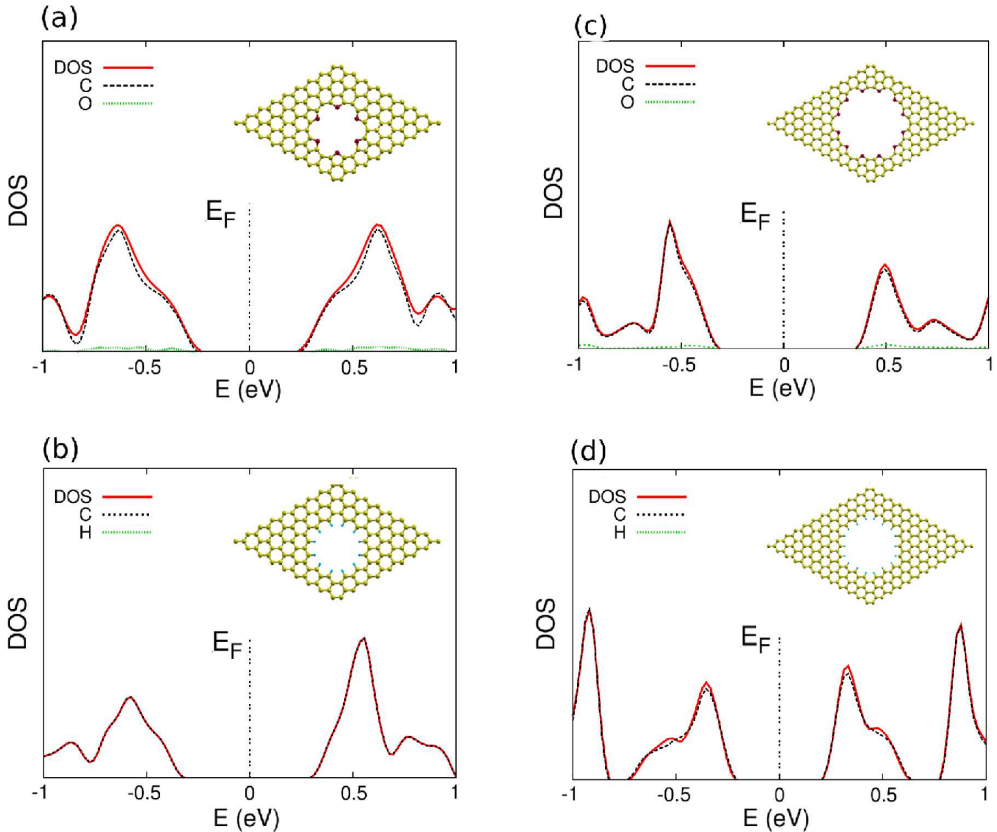


FIG. 2: DOS and PDOS of the pristine (a) O-GNM9, (b) O-GNM12, (c) H-GNM9, and (d) H-GNM12 systems. The insets show the unit cells of the relaxed structures.

Two GNM's with larger pores are shown in Fig.2(c,d). The oxygen passivated GNM, O-GNM12, has a pore diameter of ~ 1.6 nm, while the hydrogen-passivated GNM, H-GNM12, has a pore diameter of ~ 1.3 nm. The DOS of both systems indicate that they are intrinsically semiconducting, with gap sizes of 0.8 eV and 0.4 eV for the oxygen passivated and hydrogen passivated systems, respectively.

A. *n*-doping

In this section, we consider 12 *n*-doping cases of O–GNM. We will have two dopants; Li and Na, and we will consider 2 pore sizes. This allows us to study cases with multiple dopants in each pore.

We first consider the cases of O–GNM9. The pore diameter is 0.8 nm, which may spatially host up to three dopant Li or Na atoms. A lithium atom brought close to the edge of the pore (inset of Fig.3a) loses its electron to the graphene skeleton, thereby ionizing and becoming electrostatically trapped in the field of the edge dipoles, forming a Li@O–GNM9. The chemical stability of this system is estimated through a calculation of the zero temperature binding energy (E_b) of the doped crown GNM system using:

$$E_b = E_{nX@Y-GNM_c} - E_{Y-GNM_c} - E_{X_n}, \quad (1)$$

where $E_{nX@Y-GNM_c}$ is the energy of the n X-chelated Y-passivated GNM system with a $c \times c$ supercell size, E_{Y-GNM_c} is the energy of the Y-passivated GNM, and E_{X_n} is the energy of the most stable molecular cluster of n atoms of species X. We find that the binding energy of one Li atom to the pore at hand is about 1.29 eV.

The DOS and PDOS for that system is shown in Fig. 3a. The Fermi level indicates that the Li@O–GNM9 is *n*-doped. The O–GNM9 perturbs the Li state such that it raises its $2s$ state by about 1.1 eV above the Fermi level. The Li $2s$ state is therefore too far to obstruct low energy electronic transport. By integrating the DOS from the conduction band edge to the Fermi level, we find that one electron has been transferred to the O–GNM9. The binding energy of the Li atom in the pore is about 1.29 eV, and its average distance to the closest two oxygen atoms is about 2.19 Å.

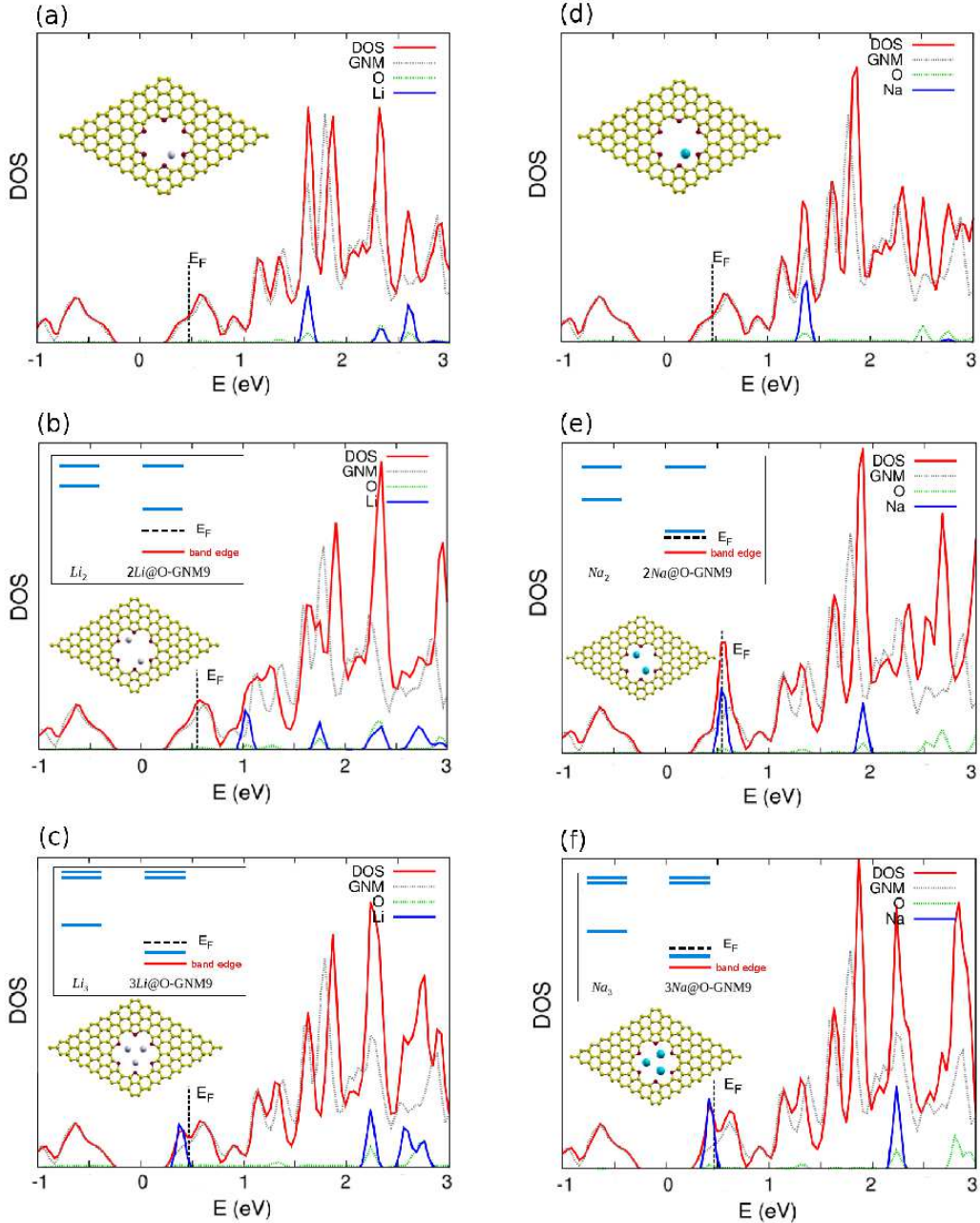


FIG. 3: Density of states of the (a) Li@O-GNM9 , (b) 2Li@O-GNM9 , (c) 3Li@O-GNM9 , and (d) Na@O-GNM9 , (e) 2Na@O-GNM9 , (f) 3Na@O-GNM9 systems (DOS). The bottom insets refer to the relaxed structures. In (b), (c), (e), and (f) the top insets show the Li/Na states within the corresponding O-GNM9 system, as compared to those of the isolated Li/Na clusters. The DOS of the pristine O-GNM9 (GNM) is shown for comparison.

We now place another lithium atom close to the pore edge. After structural relaxation the second atom docks at the pore edge opposite to the first one (inset of Fig. 3b), with a separation of 5.27 Å, and in the same plane of the GNM. The average Li distance to the closest oxygen atoms is 2.10 Å. The DOS and PDOS of the 2Li@O-GNM9 system are shown in Fig. 3b. The shift in the Fermi energy indicates the increase in the doping level of the 2Li@O-GNM9 over the Li@O-GNM9 system. Calculations confirm a charge transfer of 2e between the two lithium atoms and the graphene lattice. The DOS shows that the two *empty* Li states are now raised above the Fermi level by 0.5 eV and 1.2 eV. These two states are the positive and negative linear combinations of the atomic 2s lithium states. The binding energy of the two lithium atoms in the pore is found to be 0.79 eV. Thus the two Li atoms double the doping level, and maintain the rigid band doping picture, but with a smaller binding energy.

Adding a third lithium atom introduces a qualitative change. Whereas the states of the single Li^+ and the elongated Li_2^+ are *far* above the conduction band edge of the O-GNM9 (thus resulting in the spilling of one and two electrons to the O-GNM9, respectively), one of the states of the Li_3^+ now falls just above the conduction band edge of the O-GNM9. The O-GNM9 perturbs the Li and Li_2 spectra in such a way so as to raise their atomic/molecular HOMO states, leading to the ionization of lithium atoms in both cases. In the Li_3 case, perturbation is such that its lowest lithium 2s-like state lies just above the O-GNM9 conduction band edge, and therefore two electrons occupy that state, while the third is donated to the O-GNM9, thus doping it to a level similar to that of the Li@O-GNM9 system. The binding energy in this case is 1.91 eV. The insets of Figs. 3b and 3c show the effect the O-GNM9 has on the spectra of the Li_2 and Li_3 clusters. This *highest-load* case is probably the least desirable for device engineers, as switching the device off would involve the emptying of the lowest Li state.

The discrepancy in the binding energy of the Li atoms in the three above cases can be understood as follows: In the Li@O-GNM9 case, the cost to ionize the Li atom and to charge the O-GNM9 is compensated by the electrostatic energy gain, leading to a binding energy of 1.29 eV. The 2Li@O-GNM9 system can be thought of along the same logic; two Li atoms are now ionized in the pore, donating their electrons to the GNM, and leading to a higher electrostatic gain. This electrostatic gain is counteracted by the ionization cost of the two Li atoms, the charging of the GNM, and the electrostatic repulsion between the two

Li^+ ions, leading to a binding energy of 0.79 eV. The $3\text{Li}@\text{O-GNM9}$ case follows a different mechanism, as one of the Li_3 cluster states lies just below the Fermi level of the system. The cluster is singly ionized (Li_3^+), with its positive charge delocalized over the cluster, causing a stronger electrostatic interaction with the pore oxygen atoms compared to that between the Li^+ and its two neighboring oxygen atoms in the $\text{Li}@\text{O-GNM9}$ case, thus leading to a higher binding energy.

The situation with the Na-doping is qualitatively similar to the case of the Li-doping. Figures 3(a,b, and c) show the structure and DOS of the three systems $\text{Na}@\text{O-GNM9}$, $2\text{Na}@\text{O-GNM9}$, and $3\text{Na}@\text{O-GNM9}$. In the case of the $\text{Na}@\text{O-GNM9}$ and $2\text{Na}@\text{O-GNM9}$ systems, the $2s$ Na states are located above the Fermi level, and the systems are n -doped with a charge transfer of 1 and 2 electrons, respectively. The binding energies are 1.62 and 1.57 eV, respectively. As in the Li case, the binding energy of the $2\text{Na}@\text{O-GNM9}$ system decreases compared to the $\text{Na}@\text{O-GNM9}$ system, due to the extra charging of the GNM and the electrostatic repulsion between the two Na^+ ions. For the $3\text{Na}@\text{O-GNM9}$ system, the lowest Na_3 state lies below the Fermi energy, and hosts two of the 3Na_3 electrons, while the third electron is transferred to the GNM. The Na cluster is thus singly ionized (Na_3^+), with a binding energy of 2.79 eV. As in the Li case, the delocalized positive charge interacts with all pore oxygen atoms, leading to a higher binding energy compared to that of the $\text{Na}@\text{O-GNM9}$ system. Furthermore, the Na-doped systems have higher binding energies than the Li ones due to the higher ionization energy cost of lithium. The effect of the O-GNM9 on the spectra of the Na_2 and Na_2 clusters is sketched in the insets of Figs. 3e and 3f. As with its Li version, the $3\text{Na}@\text{O-GNM}$ should be the least interesting to device engineers.

We now turn to n -doping in the larger pores systems. We first consider the $\text{Li}@\text{O-GNM12}$, $2\text{Li}@\text{O-GNM12}$, and $3\text{Li}@\text{O-GNM12}$ systems. Figure 4 shows the structure and DOS of the three systems. The average $\text{Li}-\text{O}$ distance in the three cases is close to the case of the smaller pore. The Li^+-Li^+ distances in the $2\text{Li}@\text{O-GNM12}$ and $3\text{Li}@\text{O-GNM12}$ systems are 13.52 and 11.80 Å, respectively. The DOS of the three systems (Fig. 4) suggests that the doping level increases with the number of dopants. Indeed, calculations indicate that the charge transfer in the three cases is 1, 2, and 3 electrons, respectively. This is similar to the small pore case for the Li and Li_2 , but different for the Li_3 . Here, the 3Li atoms are ionized. The $\text{Li}@\text{O-GNM12}$ has a binding energy similar to the $\text{Li}@\text{O-GNM9}$ case. The $2\text{Li}@\text{O-GNM12}$ has a binding energy of 1.07 eV (~ 0.54 eV/dopant), higher

than the 2Li@O-GNM9, which can be mainly attributed to the smaller repulsive interaction between the two Li^+ ions, now ~ 13.5 Å apart. The 3Li@O-GNM12 system has a binding energy of 1.39 eV (~ 0.46 eV/dopant). The repulsive interaction between the 3 Li^+ ions, with a Li^+ – Li^+ distance of ~ 11.8 Å explains the lower energy per dopant compared to the 2Li@O-GNM12 case. This is different from the 3Li@O-GNM9 system, where the Li_3 cluster is singly ionized, and therefore offers a potential route for an n -doped GNM-based semiconductor.

To study the effect of increasing the doping load of the large pore systems, we study three Na-doped systems; 2Na@O-GNM12, 4Na@O-GNM12, and 6Na@O-GNM12 (Figs. 4(d, e, and f)). Two Na atoms dope the O-GNM12 with two electrons as in the O-GNM9 case. Due to the lesser repulsion between the two Na^+ ions, now 13.11 Å apart, the binding energy of the 2Na@O-GNM12 system is slightly higher (1.82 eV) than that of the 2Na@O-GNM9 one. Adding two more Na atoms (4Na@O-GNM12) to the pore leads to the formation of Na^+ ions, and hence to the doping of the O-GNM12. Calculations show that 4 electrons are transferred to the GNM. As we see in Figs. 4(d, e, and f), the O-GNM12 pulls down the lowest two states of the 4Li atoms, but they are still above the Fermi level of the system. Adding two more Na atoms (6Na@O-GNM12) leads to the lowering of one of the Na states below the Fermi level, thus achieving a doping level similar to the 4Na@O-GNM12 case. This is also the larger pore version of the 3Li@O-GNM9/3Na@O-GNM9 systems, where the highest doping load might be the least favorable when building a GNM-based device.

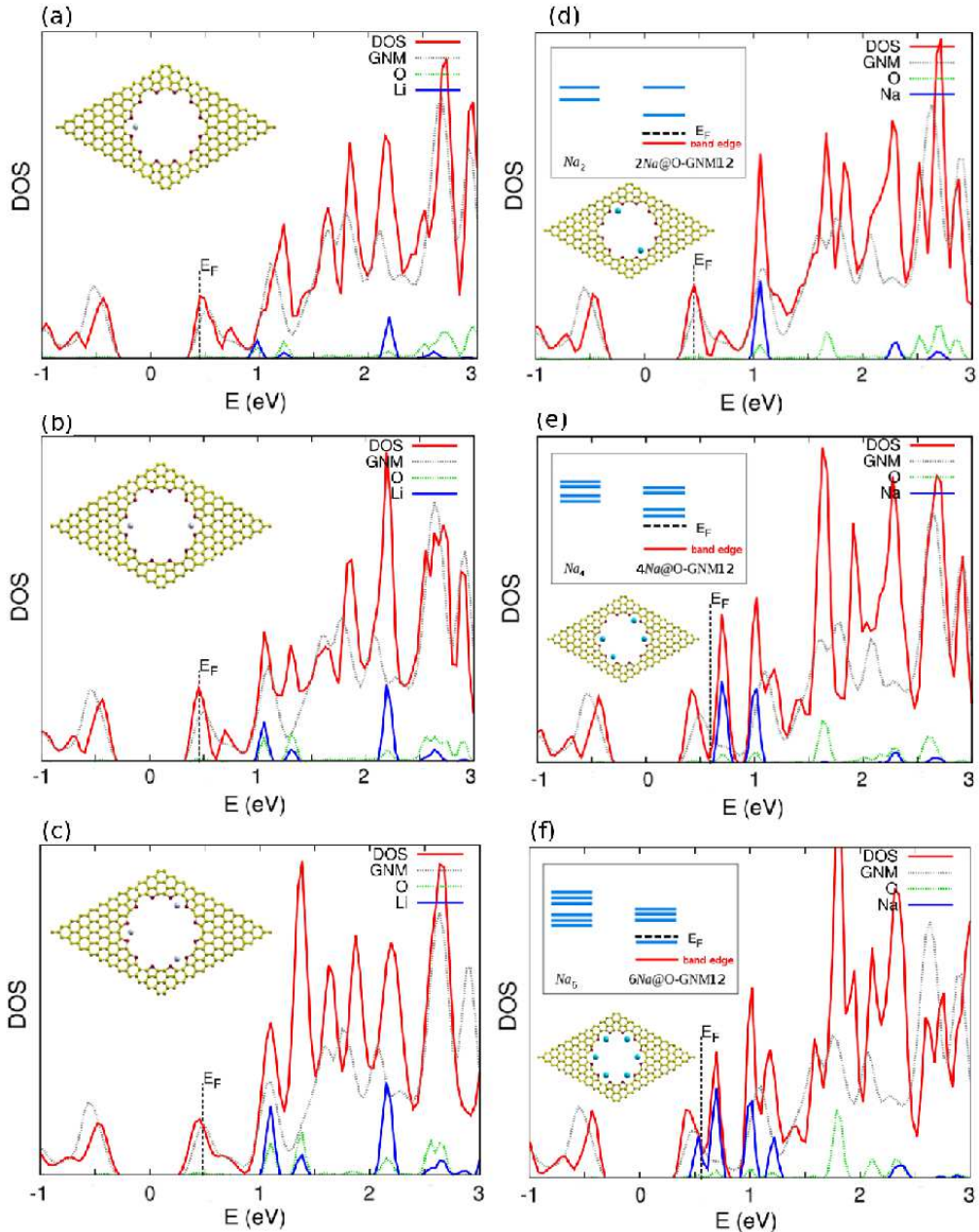


FIG. 4: Density of states of the (a) $\text{Li}@\text{O-GNM12}$, (b) $2\text{Li}@\text{O-GNM12}$, (c) $3\text{Li}@\text{O-GNM12}$, and (d) $2\text{Na}@\text{O-GNM12}$, (e) $4\text{Na}@\text{O-GNM12}$, (f) $6\text{Na}@\text{O-GNM12}$ systems (DOS). The bottom insets refer to the relaxed structures. In (d), (e), and (f) the top insets show the Li/Na states within the corresponding O-GNM12 system, as compared to those of the isolated Li/Na clusters. The DOS of the pristine O-GNM12 (GNM) is shown for comparison.

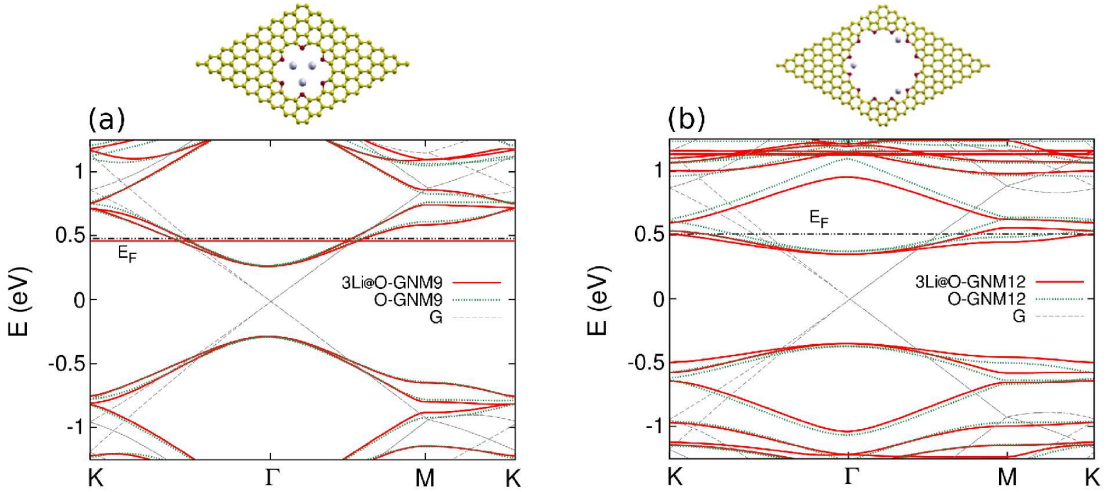


FIG. 5: Electronic band structures of (a) 3Li@O-GNM9, and (b) 3Li@O-GNM12. The band structure of graphene, pristine O-GNM9, and O-GNM12 are shown for comparison.

To confirm the rigid band nature of the doping, we show the band structures of two n -doped systems; 3Li@O-GNM9 (Fig.5a), and 3Li@O-GNM12 (Fig.5b). Compared to the undoped O-GNMs, there is no significant change in the band curvatures in the Fermi level/gap region. The pristine graphene is also shown for comparison. The bands are linear in the vicinity of the Fermi energy, with a group velocity of about half/quarter that of graphene for the O-GNM9/O-GNM12. The results of the n -doping O-GNM structures are shown in table.I

System	E_b (E_b/n)	d_{X-O}	System	E_b (E_b/n)	d_{X-O}
Li@O-GNM9	1.29 (1.29)	2.19	Na@O-GNM9	1.62 (1.62)	2.36
2Li@O-GNM9	0.79 (0.40)	2.10	2Na@O-GNM9	1.57 (0.79)	2.33
3Li@O-GNM9	1.91 (0.95)	2.08	3Na@O-GNM9	2.79 (1.40)	2.44
Li@O-GNM12	1.30 (1.30)	2.2	2Na@O-GNM12	1.82 (0.91)	2.33
2Li@O-GNM12	1.07 (0.54)	2.18	4Na@O-GNM12	2.41 (1.21)	2.30
3Li@O-GNM12	1.39 (0.46)	2.17	6Na@O-GNM12	2.55 (0.85)	2.36

TABLE I: Binding energies (E_b (eV)), binding energies per dopant (E_b/n (eV)), and average distance between a dopant and the nearest oxygen atoms (d_{X-O} (Å)) of various n -doping systems.

B. *p*-doping

We now examine *p*-doping of large pore GNM systems. We consider 4 doped H–GNM9 systems (pore size 0.9 nm), and 4 doped H–GNM12 systems (pore size 1.2 nm), using F and Cl. The reported binding energies are calculated from the energies of the most stable form (F_2 and Cl_2 molecules).

A fluorine atom brought close to the edge of the H–GNM9 pore will have its spectrum perturbed by the pore dipoles, resulting in the LUMO of the F falling below the valence band edge of the GNM. This will cause an electron to spill from the GNM skeleton to occupy the F LUMO, thus ionizing it, and *p*-doping the GNM. The electrostatic attraction between the F anion and the nearby hydrogen creates an ultra stable environment for the F anion. Figure 6a shows the structure of the F@H–GNM9. The average F–H distance is 1.73 Å. The binding energy of F@H–GNM9 is found to be 2.80 eV. The H–GNM causes the F $2p_z$ state to be pinned about 0.3 eV below the valence band edge of the H–GNM, and 0.1 eV below the Fermi level. Integrating the DOS from the valence band edge to the Fermi level indicates that one electron has been transferred to H–GNM9.

Adding another F atom to the system leads to a similar picture, with the second F atom pinned across the pore from the first one (Fig. 6, inset), with an average F–H distance of 1.73 Å. The binding energy of the 2F@H–GNM9 system is found to be 1.72 eV. The decrease in the binding energy per dopant can be partially attributed to the electrostatic repulsion between the two fluorine anions.

The DOS of the 2F@H–GNM9 system is shown in Fig. 6b. The GNM is *p*-doped, with the Fermi energy located \sim 0.3 eV below the valence band edge. The two F atoms are now ionized, with their $2p_z$ states full, and located \sim 0.2 eV *below* the Fermi level, and hence will not interfere with electronic transport of a 2F@H–GNM9-based device.

The situation with the second *p*-dopant, chlorine, is slightly different. Doping with one Cl atom leads to qualitatively similar results. A Cl@H–GNM9 has a Cl–H distance of 2.44 Å, with a binding energy of 1.84 eV (Fig. 6c). The DOS of the system shows that the now-filled p_z state of the Cl is located 0.1 eV below the Fermi level, which is pinned 0.2 eV below the edge of the valence band. Upon adding another Cl atom, the system favors the formation of an *elongated* Cl_2 molecule (Cl_2^*), which sticks out of the plane of the GNM (Fig. 6d). The Cl_2^* molecule has a Cl–Cl distance of 2.28 Å, larger than the Cl_2 molecular distance

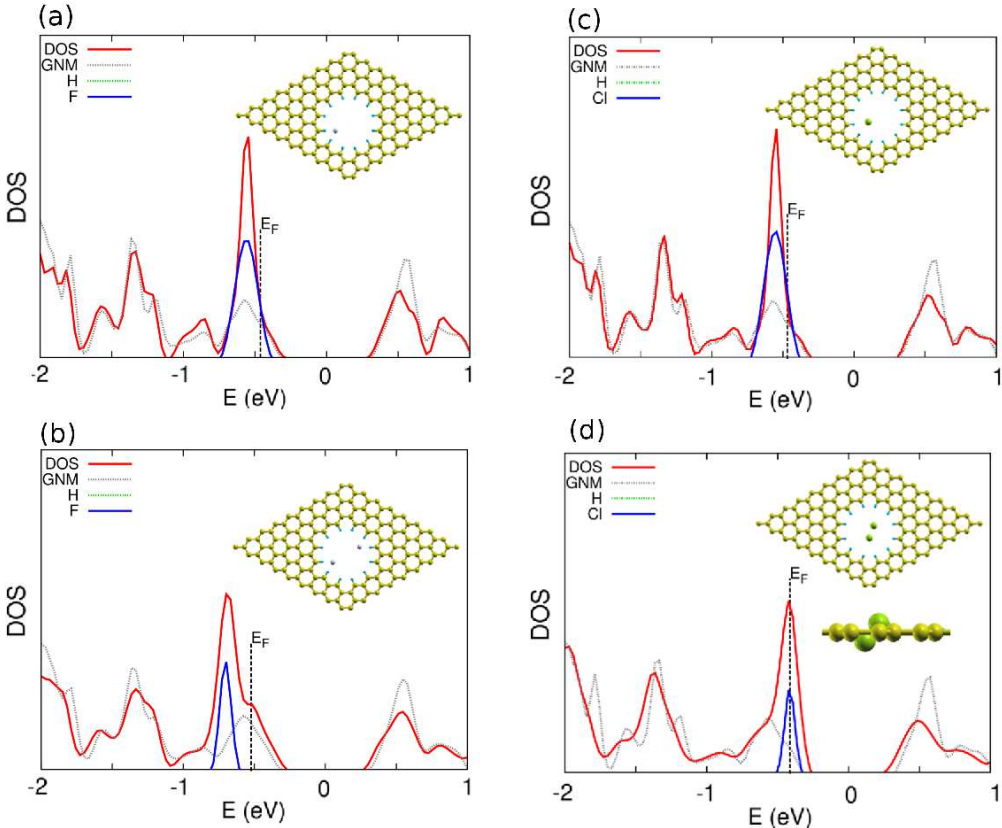


FIG. 6: Density of states of the (a) F@H-GNM9, (b) 2F@H-GNM9, (c) Cl@H-GNM9, and (d) 2Cl@H-GNM9 systems (DOS). The inset figures refer to the relaxed structures. In (d) the lower inset shows a side view of the 2Cl@H-GNM9 system indicating the off-plane structure of the 2Cl cluster. The DOS of the pristine H-GNM9 (GNM) is shown for comparison.

of 2.00 Å. The DOS of the system shows that the GNM is slightly doped and that the Cl p_z states are only partially full. The Löwdin charge analysis confirms this picture showing that the Cl₂* molecule carries a negative charge of about 0.2e. Adding more dopants does not lead to stable structures, so the maximum load for the considered H-GNM9 pore is two dopants.

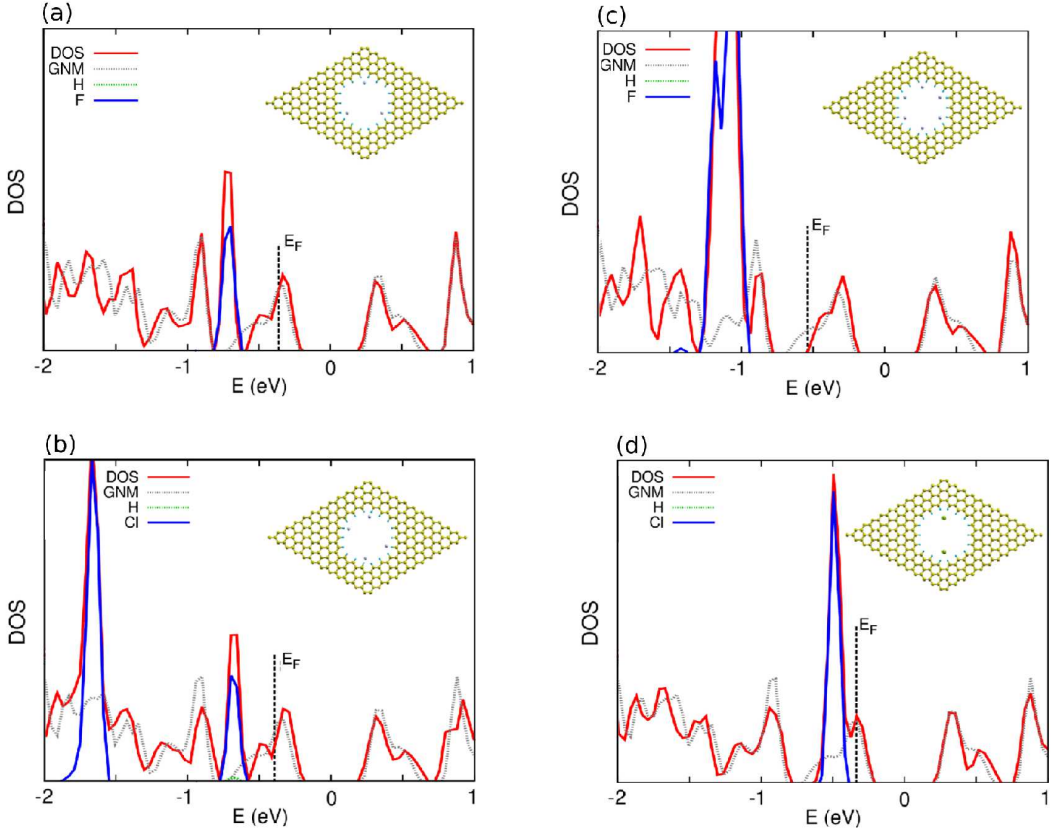


FIG. 7: Density of states of the (a) 3F@H-GNM12, (b) 4F@H-GNM12, (c) 6F@H-GNM12, and (d) 2Cl@H-GNM12 systems (DOS). The inset figures refer to the relaxed structures. The DOS of the pristine H-GNM12 (GNM) is shown for comparison.

Next we describe our *p*-doping results for larger pores. We form a hydrogen doped GNM with a pore radius of about 1.3 nm, H-GNM12. Since the pore is large, and two fluorine atom successfully doped the smaller pore system, we begin with a three fluorine system, 3F@H-GNM12 (Fig. 7a) The average distance between the fluorine and the closest two hydrogen atoms in the structurally relaxed system is 1.65 Å. The average F-F distance is 8.62 Å. The DOS of the system shows that the GNM12 is *p*-doped, with the Fermi energy placed ~ 0.4 eV below the valence band edge. The fluorine $2p_z$ states are all full, and are located at least 0.3 eV below the Fermi level, indicating the full ionization of the three fluorine dopants. The integrated DOS shows that the GNM lost three electrons. The binding energy of the 3F@H-GNM12 is 3.72 eV.

Adding more fluorine atoms leads to similar physics. For the 4F@H-GNM12 case (Fig.

7b), doping occurs with 4 electrons. The smallest average F–F distance is 5.97 Å. The Fermi level sinks deeper in the valence band, 0.2 eV from the band edge. The fluorine $2p_z$ states are all populated, and the closest one to the Fermi level is 0.4 eV away. The binding energy of the 4F@H–GNM12 system drops to 3.08 eV. For the 6F@H–GNM12 system, the smallest average F–F distance drops to 5.04 Å. The highest filled fluorine $2p_z$ state is ~ 0.3 eV away from the Fermi level, which is pinned 0.4 eV below the valence band edge. The binding energy of the 6F@H–GNM12 is 4.87 eV. Calculations show that the charge transfer from the GNM to the fluorine atoms is $4e$ for the 4F@H–GNM12 and $6e$ for the 6F@H–GNM12, confirming the full ionization of the fluorine atoms in both systems. The average F–H distance in the 4F@H–GNM12 system is 1.21 Å while it is 1.61 Å in the 3F@H–GNM12 and the 6F@H–GNM12 systems. This difference can be attributed to the breaking of the rotational symmetry of the pore by the 4F dopants structure, where each fluorine atom faces one hydrogen. In the 6F@H–GNM12 case, each fluorine atom faces two hydrogen atoms.

Replacing F by Cl in the large pore leads to different physics. Studying the 2Cl@H–GNM12 systems shows that a stable structure can be achieved with the 2Cl atoms docked at opposite sides of the pore at 8.46 Å apart (Fig. 7d). The DOS shows that the system is *p*-doped, with the Fermi level 0.2 eV below the band edge, and that the *filled* Cl $3p_z$ states are right below the Fermi energy, indicating the full ionization of the Cl atoms. Although the system is stable, the configuration with the separated Cl₂ molecule and H–GNM12 is energetically favorable by 0.07 eV. The lesser binding energies of the Cl-doped GNMs compared to the F-doped ones are due to the higher binding energy of the Cl₂ molecule (2.52 eV for Cl₂ vs 1.64 eV for F₂). Unlike the *n*-doping case, the highest doping load is favorable when building a GNM-based device.

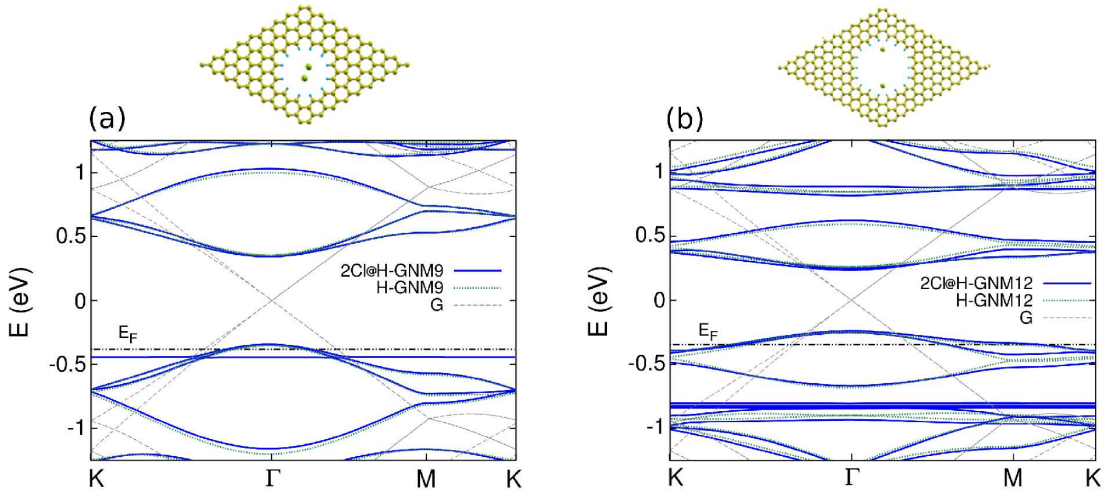


FIG. 8: Electronic band structures of (a) 2Cl@H-GNM9, and (b) 2Cl@H-GNM12. The band structure of graphene, pristine H-GNM9, and H-GNM12 are shown for comparison.

Chelation *p*-doping of GNM s occurs in a rigid band manner. This is clear from the inspection of the band structure of the doped systems. In Fig. 8, we show the band structures of the 2Cl@H-GNM9 and 2Cl@H-GNM12 systems. Band curvatures are very similar to those of the pristine GNM systems. In addition, they are linear in the neighborhood of the Fermi level, with an electronic group velocity half/quarter that of graphene for the H-GNM9/H-GNM12. Table II summarizes our results for the *p*-doped systems.

System	E_b (E_b/n)	d_{X-H}	System	E_b (E_b/n)	d_{X-H}
F@H-GNM9	2.80 (2.80)	1.70	Cl@H-GNM9	1.84 (1.84)	2.44
2F@H-GNM9	1.72 (0.86)	1.71	2Cl@H-GNM9	-0.19 (-0.085)	3.09
3F@H-GNM12	3.70 (1.85)	1.66	2Cl@H-GNM12	-0.07 (-0.035)	2.37
4F@H-GNM12	3.08 (0.77)	1.23			
6F@H-GNM12	4.87 (0.81)	1.60			

TABLE II: Binding energies (E_b (eV)), binding energies per dopant (E_b/n (eV)), and average distance between a dopant and the nearest hydrogen atoms (d_{X-H} (Å)) of various *p*-doping systems.

C. Conclusion

Graphene nanomeshes (GNM's) with experimentally feasible pores (> 1 nm) have band gaps and electronic mobilities that are attractive for nanoelectronic applications. We use first-principles calculations to show that it is possible to achieve stable controlled doping of large-pore GNM's using multiple ion chelation. Selective passivation of the pore edges allows for the hosting of negative and positive ions. Stable n -doping of a 0.8 nm pore GNM using multiple dopants is energetically favorable using Li, Li_2 , and Li_3 clusters, with a binding energy that is higher than $50k_B T$ at room temperature. Similar results have been obtained with Na in the same pore. For larger pores (~ 1.3 nm), more dopants can be loaded into the pore, with a binding energy in the same order. The doping level increases with the number of dopants, and occurs in a rigid band way, except when at the maximum dopant load, where the hybridization occurring between the valence s states of the multiple dopants is such that the lowest hybridized state falls below the Fermi level of the system, hence getting populated by the dopant electrons.

For the case of p -doping, we find that stable rigid band doping occurs with two F atoms in the first hydrogen-passivated pore. Whereas 2Cl atoms p -dope the H-GNM, the binding energy of the system comparable to that of the Cl_2 molecule. The larger pore systems also favors Fluorine as a dopant, where 6F^- ions can be stably hosted, while the 2Cl systems still exhibits a binding energy close to the Cl_2 molecule due to its high molecular binding energy. Our results satisfy the need to study relatively large systems with bigger pores, and more ions per pore, which renders GNM's closer to an experimentally realizable device in terms of length scale.

D. Computational Methods

Electronic structure calculations were performed with the Quantum Espresso software package ⑧. Minimum energy configurations were obtained by relaxing the X@Y-GNM_c systems with forces less than 0.001 Ry/Bohr. The calculations were performed on up to 16 nodes of the Biblioteca Alexandrina supercomputer using the generalized gradient approximation PBE functional,²⁸ with an energy cutoff of 45 Ry, a $12 \times 12 \times 1$ Monkhorst-Pack k-point grid for the X@Y-GNM₉ systems, and a $6 \times 6 \times 1$ k-point grid for the larger X@Y-

GNM12 ones. A vacuum distance of 12 Å has been used for an image separation in the direction perpendicular to the plane of the GNM. Charge transfer is calculated by integrating the total density of states.

Acknowledgment

This work was supported in part by the Center for Fundamental Physics, Zewail City of Science and Technology. The authors would also like to acknowledge the support of the supercomputing facility at the Bibliotheca Alexandrina, Alexandria, Egypt.

- ¹ H. Du, J. Li, J. Zhang, G. Su, X. Li, and Y. Zhao, *The Journal of Physical Chemistry C* **115**, 23261 (2011).
- ² B. F. Machado and P. Serp, *Catal. Sci. Technol.* **2**, 54 (2012).
- ³ Y. Wu, Y.-M. Lin, A. A. Bol, K. A. Jenkins, F. Xia, D. B. Farmer, Y. Zhu, and P. Avouris, *Nature* **472**, 74 (2011).
- ⁴ C. Sire, F. Ardiaca, S. Lepilliet, J.-W. T. Seo, M. C. Hersam, G. Dambrine, H. Happy, and V. Derycke, *Nano Letters* **12**, 1184 (2012).
- ⁵ Y.-M. Lin, K. A. Jenkins, A. Valdes-Garcia, J. P. Small, D. B. Farmer, and P. Avouris, *Nano Letters* **9**, 422 (2009).
- ⁶ Y. M. Lin, C. Dimitrakopoulos, K. A. Jenkins, D. B. Farmer, H. Y. Chiu, A. Grill, and P. Avouris, *Science* **327**, 662 (2010).
- ⁷ K. Bolotin, K. Sikes, Z. Jiang, M. Klima, G. Fudenberg, J. Hone, P. Kim, and H. Stormer, *Nature* **451**, 351 (2008).
- ⁸ J. A. Fürst, J. G. Pedersen, C. Flindt, N. A. Mortensen, M. Brandbyge, T. G. Pedersen, and A.-P. Jauho, *New Journal of Physics* **11**, 095020 (2009).
- ⁹ T. Pedersen, C. Flindt, J. Pedersen, N. Mortensen, A.-P. Jauho, and K. Pedersen, *Physical Review Letters* **100**, 1 (2008).
- ¹⁰ W. Liu, Z. F. Wang, Q. W. Shi, J. Yang, and F. Liu, *Physical Review B* **80**, 2 (2009).
- ¹¹ R. Petersen and T. Pedersen, *Physical Review B* **80**, 1 (2009).
- ¹² M. Vanević, V. Stojanović, and M. Kindermann, *Physical Review B* **80**, 1 (2009).

¹³ R. Martinazzo, S. Casolo, and G. Tantardini, *Physical Review B* **81**, 1 (2010).

¹⁴ A. Baskin and P. Král, *Scientific reports* **1**, 36 (2011).

¹⁵ R. Petersen, T. G. Pedersen, and A.-P. Jauho, *Acs Nano* **5**, 523 (2010).

¹⁶ M. M. Fadlallah, A. A. Maarouf, U. Schwingenschlögl, and U. Eckern, *Journal of physics. Condensed matter : an Institute of Physics journal* **29**, 055301 (2016), ISSN 1361-648X, URL <http://www.ncbi.nlm.nih.gov/pubmed/27911883>.

¹⁷ A. A. Maarouf, R. A. Nistor, A. Afzali-Ardakani, M. A. Kuroda, D. M. Newns, and G. J. Martyna, *Journal of Chemical Theory and Computation* **9**, 2398 (2013).

¹⁸ J. Bai, X. Zhong, S. Jiang, Y. Huang, and X. Duan, *Nature nanotechnology* **5**, 190 (2010).

¹⁹ J. Ding, K. Du, I. Wathuthanthri, C.-H. Choi, F. T. Fisher, and E.-H. Yang, *Journal of Vacuum Science & Technology B* **32**, 06FF01 (2014).

²⁰ J. Zhang, H. Song, D. Zeng, H. Wang, Z. Qin, K. Xu, A. Pang, and C. Xie, *Scientific Reports* **6** (2016).

²¹ M. König, G. Ruhl, J.-M. Batke, and M. C. Lemme, *Nanoscale* **8**, 15490 (2016).

²² J. Guo, J. Lee, C. I. Contescu, N. C. Gallego, S. T. Pantelides, S. J. Pennycook, B. A. Moyer, M. F. Chisholm, C. J. Pedersen, Z. Grote, et al., *Nature Communications* **5**, 5389 (2014).

²³ P. W. Anderson, *Phys. Rev.* **124**, 41 (1961).

²⁴ D. M. Newns, *Phys. Rev.* **178**, 1123 (1969).

²⁵ B. Hammer and J. K. Norskov, *Nature* **376**, 238 (1995).

²⁶ R. A. Nistor, D. M. Newns, and G. J. Martyna, *ACS nano* **5**, 3096 (2011).

²⁷ A. C. Hewson and D. M. Newns, *Japanese Journal of Applied Physics* **2S2**, 121 (1974).

²⁸ J. P. Perdew, K. Burke, and M. Ernzerhof, *Phys. Rev. Lett.* **77**, 3865 (1996).